

15058 PORPHYRITIC-SUBOPHITIC QUARTZ-NORMATIVE ST.8 2672.0 g  
MARE BASALT

**INTRODUCTION:** 15058 is a coarse-grained and vuggy quartz normative basalt containing pigeonite phenocrysts up to 2 cm long. It crystallized approximately 3.3 or 3.4 b.y. ago.

The rock was collected about 30 m east-northeast of the ALSEP central station. No other rocks as big as 15058 occur in the area (Fig. 1). It was less than one-fourth buried, and lacked fillets or dust. It is olive-gray, tough, blocky, and angular (Fig. 2), with a few zap pits.

**PETROLOGY:** 15058 is readily classified as a member of the Apollo 15 quartz-normative group of basalts: macroscopically it has abundant greenish pyroxene phenocrysts 1 to 2 cm long, and lacks olivine phenocrysts. Diktytaxitic vugs, acicular plagioclases (some with radiate patterns) (Fig. 3), and interstitial brown mafic grains and opaque phases are conspicuous. Thin sections (Figs. 4, 5) show the prominent complexly-zoned and twinned pigeonite phenocrysts, plagioclase laths and plates which evidently grew with hollow cores, and interstitial pyroxene, mesostasis, opaque phases, and cristobalite. Radiate structures are common, and rare relict olivines are surrounded by pigeonite.

The sample has always been classified as a quartz-normative basalt, under the different names used for that group; e.g. Brown et al. (1972a) call it a "pyroxene-rich, tridymite gabbro" of their Mare Basalt Type 1. Most petrographic reports have been restricted in scope but short general descriptions were given by Gay et al. (1972) and Juan et al. (1972). Pyroxenes have received most attention. They contain inclusions, including spinels and Ni-iron, and exsolved platelets. Microprobe analyses of the pyroxenes (Gay et al., 1972; Morawski et al., 1972; Papike et al., 1972; and Bence and Papike, 1972) are summarized in Figure 6 and Table 2. Cores of Mg-pigeonite ( $\text{En}_{68}\text{Wo}_5$ ) are zoned to  $\sim\text{En}_{43}\text{Wo}_{17}$ , then mantled by sub-calcic augite which is also zoned ( $\text{En}_{43}\text{Wo}_{33}$  to  $\text{En}_{34}\text{Wo}_{36}$ ). The pyroxenes in the cores of plagioclase are distinct ( $\text{En}_{38}\text{Wo}_{14}$ ) according to Gay et al. (1972), who also did not find pyroxferroite (although Grove and Bence, 1978 refer to the existence of pyroxferroite in 15058, and Papike et al., 1972, and Bence and Papike, 1972, show an analysis close to pyroxferroite in composition). Bence and Papike (1972) discuss minor element trends, noting a sharp increase in Ti/Al to  $\sim 1/2$  (corresponding to a drop in Al) when augite enters the crystallization sequence. Exsolution is visible under the microscope, and was studied by single-crystal x-ray diffraction (Gay et al. 1972; Papike et al., 1972) and TEM (Grove, 1982) methods. Papike et al. (1972) stress that the pigeonite cores do not show exsolution (Fig. 7). The exsolution features are consistent with slow cooling (Papike et al. 1972; Grove, 1982). Bence and Papike (1972) also note that the phenocrysts have no regular forms and may

be resorbed. Mossbauer studies by Burns et al. (1973), made possible because of the large phenocrysts, show negligible  $\text{Fe}^{3+}$  and  $\text{Cr}^{2+}$ , but significant  $\text{Cr}^{3+}$  and  $\text{Ti}^{3+}$ , as well as  $\text{Fe}^{2+}$ . Absorption spectral measurements also failed to show  $\text{Fe}^{3+}$ . Morawski et al. (1972) did Mossbauer studies, on hand-separated pyroxenes, finding that  $\text{Fe}^{2+}$  site preference differed in pigeonite and augite. They also did not detect  $\text{Fe}^{3+}$ , but also did not find  $\text{Ti}^{3+}$  in their polarized absorption spectra. Abu-Eid et al. (1973) did not find  $\text{Fe}^{3+}$ , did find  $\text{Ti}^{3+}$  in rims,  $\text{Cr}^{3+}$  in core pigeonites, and probably no  $\text{Cr}^{2+}$  in pyroxene. They depict their absorption spectra for a 15058 zoned pyroxene. The characteristics of pyroxene nucleation density, size and trace element zoning trends, and exsolution, have been extensively used in deciphering the cooling history of 15058 (below).

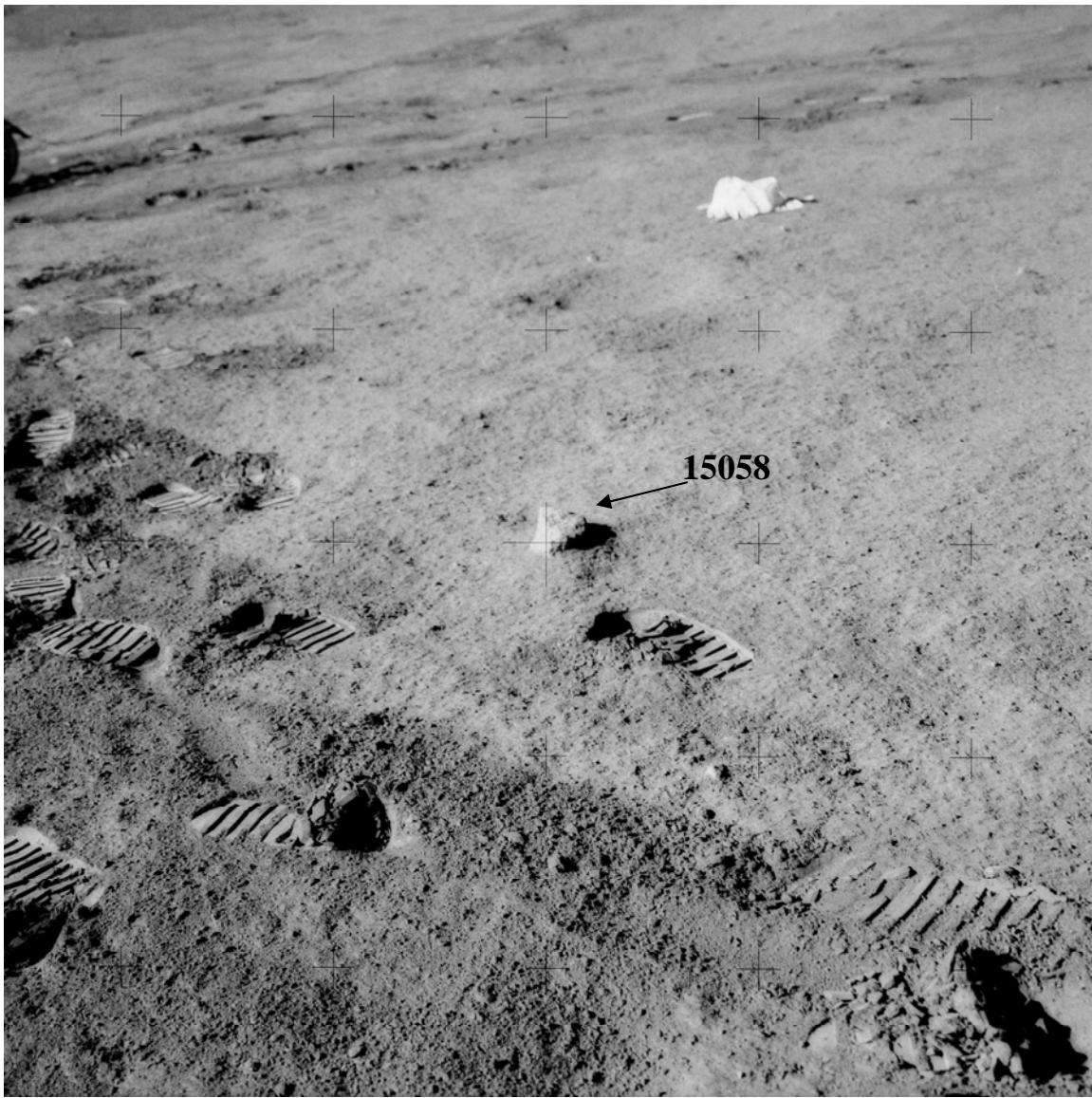


Figure 1. AS-15-92-12411



Figure 2. Pre-split. S-71-44205

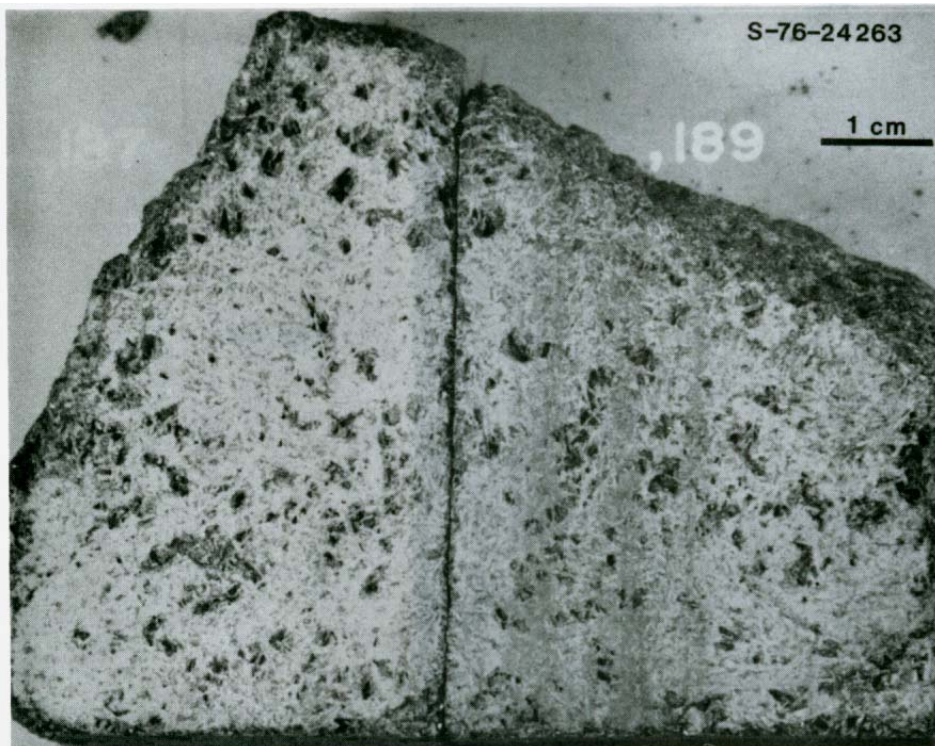


Figure 3. Diktytaxitic texture in sawn faces. S-76-24263



Figure 4. Whole thin section 15058,130.

TABLE 15058-1. Modes of 15058

Reference	Cpx	Pl	Opq	Crist	Meso	Ol	Tr/Fe
AlS Info. Cat. (1971)	71*	24	2-3	1	1	tr	<0.6
Rhodes and Hubbard (1973)	68.3	27.1	3.5	1.5	0.6	1.8	0.3
Juan <i>et al.</i> (1972)	72	22	2	3			<1

(a) 56% phenocrysts, 15% groundmass



Fig. 5a

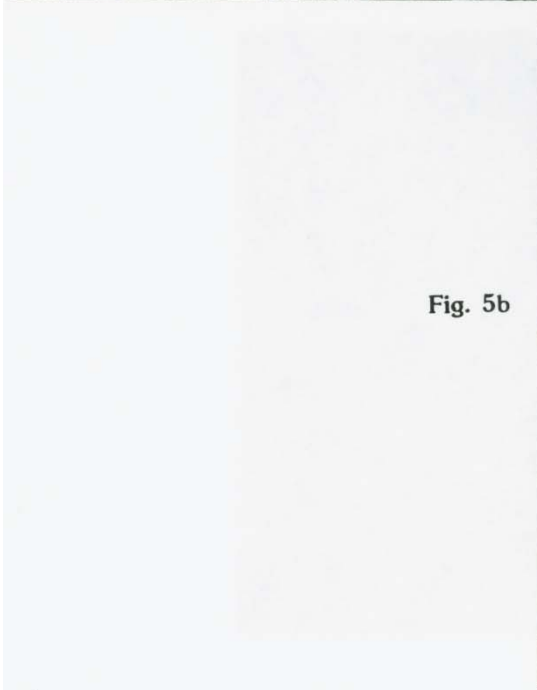


Fig. 5b

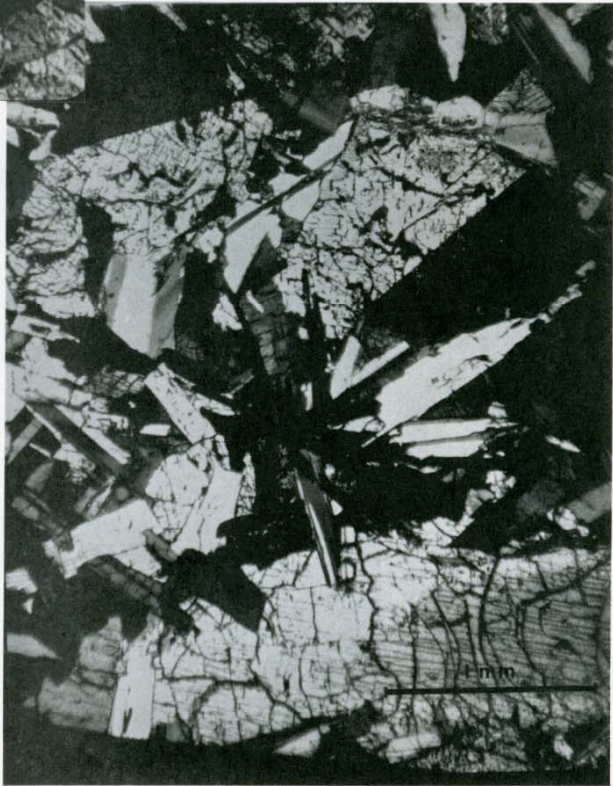




Fig. 5c

Figure 5. Photomicrographs of 15058,130, all crossed polarizers.  
(a) olivine phenocryst and lathy hollow plagioclases;  
(b) radiate growth of plagioclase, pigeonite twins;  
(c) twinned, zoned pigeonite phenocrysts.

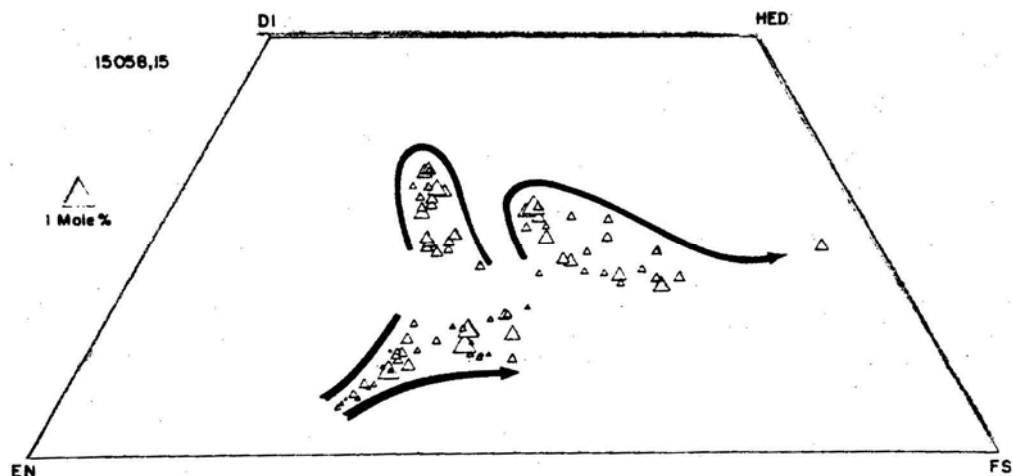


Figure 6. Compositions of pyroxenes (Papike et al., 1972).

TABLE 15058-2. Representative microprobe analyses of pyroxenes in 15058 (Bence and Papike, 1972)

	1	2	3	4	5	6	7	8	9	10	11
SiO <sub>2</sub>	52.0	50.9	51.4	52.5	51.7	51.3	50.7	50.4	48.2	51.6	51.5
Al <sub>2</sub> O <sub>3</sub>	2.01	3.95	1.81	3.07	2.41	2.81	2.07	1.31	1.43	2.47	2.77
TiO <sub>2</sub>	0.53	0.58	0.40	0.61	0.65	0.71	0.66	0.84	1.11	0.73	0.63
FeO	23.4	22.1	24.2	18.8	18.1	23.7	23.8	27.0	30.2	15.4	14.5
MgO	15.3	15.6	15.4	17.9	14.6	14.0	13.9	10.4	7.41	14.4	14.2
CaO	5.24	6.50	5.37	6.14	11.1	7.40	7.46	9.80	10.8	14.1	14.7
Na <sub>2</sub> O	0.0	0.0	0.0	0.05	0.06	0.02	0.01	0.01	0.03	0.04	0.03
Cr <sub>2</sub> O <sub>3</sub>	0.86	0.58	0.66	1.18	1.14	0.93	0.74	0.54	0.45	1.05	1.06
	99.3	100.2	99.2	100.3	99.8	100.9	99.3	100.3	99.6	99.8	99.4
Si	1.982	1.921	1.973	1.946	1.953	1.943	1.956	1.969	1.942	1.943	1.941
Al <sup>IV</sup>	0.018	0.079	0.027	0.054	0.047	0.057	0.054	0.031	0.058	0.057	0.059
Al <sup>VI</sup>	0.072	0.097	0.055	0.080	0.060	0.068	0.040	0.029	0.010	0.053	0.064
Ti	0.015	0.017	0.012	0.017	0.018	0.020	0.019	0.025	0.034	0.021	0.018
Fe	0.745	0.698	0.778	0.584	0.571	0.752	0.769	0.882	1.017	0.486	0.458
Mg	0.872	0.875	0.879	0.990	0.824	0.790	0.798	0.606	0.444	0.805	0.798
Ca	0.214	0.263	0.221	0.244	0.447	0.300	0.309	0.410	0.464	0.568	0.594
Na	0.000	0.000	0.000	0.004	0.004	0.002	0.001	0.000	0.002	0.003	0.002
Cr	0.026	0.017	0.020	0.035	0.034	0.028	0.022	0.017	0.014	0.031	0.031

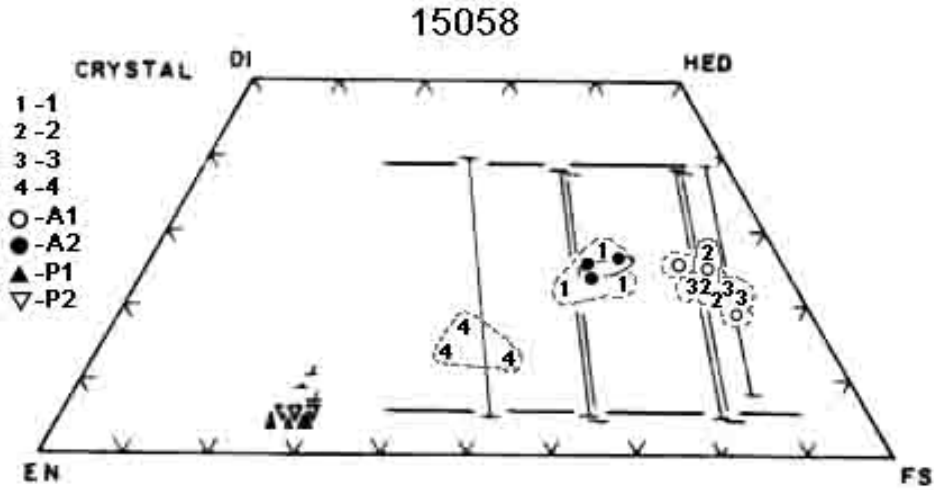


Figure 7. Pyroxene exsolutions (Papike et al., 1972).

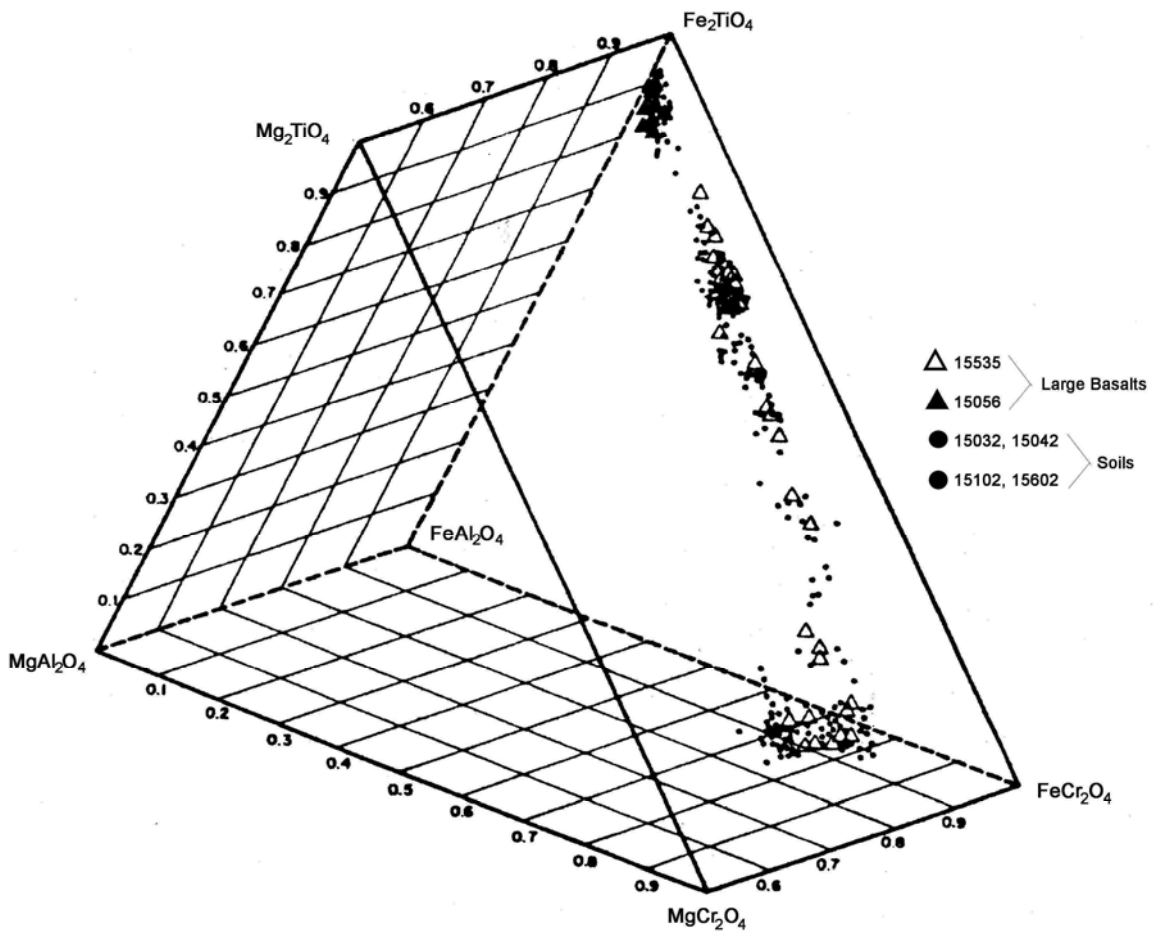


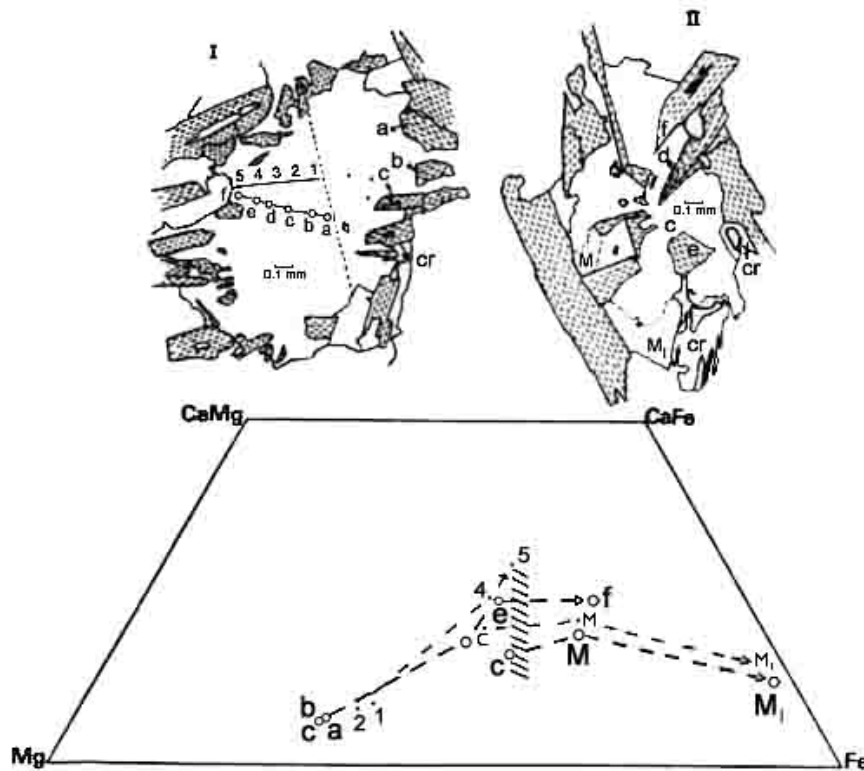
Figure 8. Spinel compositions (Haggerty, 1972d)

According to Gay et al. (1972) plagioclases are  $\sim\text{An}_{90}$  and are unzoned, with x-ray diffraction showing transitional anorthite structures. Some have rectangular cores of Fe-pigeonite, which are probably trapped because there is no orientation relationship. In contrast, Juan et al. (1972) report that the composition of the plagioclase is  $\text{An}_{78}$ . Wenk et al. (1973) report  $\text{An}_{89}$ , and describe antiphase b-domains found in their TEM studies, as well as submicroscopic structures which characterize the beginning of exsolution. They did not observe c-domains.

Haggerty (1972b,c) reported studies of the spinel series; 15058 contains only Cr-Al-ulvospinel (Fig. 8). Taylor and McCallister (1972a,b) and Taylor et al. (1972) analyzed Zr in ilmenite and ulvospinel to elucidate the thermal history (below). Roedder and Weiblen (1972) observed late immiscible high-Si and high-Fe melt inclusions in 15058 but report no data. Engelhardt (1979) inferred a paragenesis of  $\text{plag} \rightarrow \text{ilm} \rightarrow \text{px}$  from ilmenite textural relations, which contrast with other workers' conclusions that pyroxene is the obvious first-crystallizing phase. Drever et al. (1973) and Donaldson et al. (1977) published the same diagram (Fig. 9) illustrating subophitic/ophitic textural relationships between pyroxenes and plagioclase as well as chemical trends (microprobe data) in a discussion of radiate structures, but did not specifically discuss the diagram or 15058. Simmons et al. (1975) studied microcracks, using techniques which essentially determine the pressures at which cracks close. A large proportion of the cracks in 15058 close at  $\sim 300$  bars. Simmons et al. (1975) illustrate sigmoidal cracks in matrix pyroxenes, and state that they are probably from the same process that produced curved cracks in phenocrysts. Huffman et al. (1972, 1974) tabulate magnetic and Mossbauer data obtained to elucidate the state and distribution of iron: no metal was detected in the Mossbauer study but a very small amount, 0.058%, was revealed in the magnetic studies. 98.6% of the  $\text{Fe}^{2+}$  resides in pyroxene, 1.4% in ilmenite, and no olivine was detected.

Cooling rate: Thermal histories have been deduced from mineralogical and textural characteristics, in many cases using the results of experimental studies for comparison. Bence and Papike (1972) preferred a two-stage cooling history, the first fast while phenocrysts crystallize, the second slower during plagioclase crystallization. Taylor and McCallister (1972a,b) used the distribution of Zr between ilmenite and ulvospinel to deduce thermal aspects, concluding that Zr was "quenched in" at a high temperature compared with other rocks. Lofgren et al. (1975), with a direct comparison of phenocryst morphologies and rock textures with the products of experiments run at known linear cooling rates, concluded that both phenocrysts and matrix cooled at  $< 1^\circ\text{C/hr}$ . Grove and Walker (1977) used an experimental study on (the near isochemical) 15597 as a basis for comparison of pyroxene nucleation density (Fig. 10) to deduce an early rate of  $0.04^\circ\text{C}-0.2^\circ\text{C/hr}$ ., and from plagioclase size (Fig. 11) deduced a later rate of  $\sim 0.1^\circ\text{C/hr}$ , i.e., roughly linear. They caution that no real significance could in any case be attached to differences between deduced early and late-stage cooling rates for such coarse basalts, and their slowest experiments ( $0.5^\circ\text{C/hr}$ ) did not quite reproduce the crystal sizes of the rock. They calculate that 15058 crystallized at least 300 cm from a conductive boundary. Grove and Bence (1977) used the minor element chemistry of pyroxenes produced in the same experiments as a basis for comparison with natural 15058 data. 15058 pigeonite cores are similar to those produced in  $3.75^\circ\text{C/hr}$ , but the absolute rates are not well-

constrained. 15058 cooled rapidly enough for plagioclase nucleation to be suppressed, but probably less than  $0.5^{\circ}\text{C/hr}$ . Grove (1982) used a "lamellae coarsening speedometer" for exsolution, using TEM techniques, comparable with grain size-based cooling rate estimates. Pyroxene microlites have structures similar to those in slow cooling-rate experiments. An integrated cooling rate of  $\sim 0.02^{\circ}\text{C/hr}$  is similar to that derived from plagioclase data (Walker et al., 1977) which gave  $0.1^{\circ}\text{C/hr}$  from  $\sim 1050^{\circ}\text{C}$  to  $950^{\circ}\text{C}$ , from which a  $300^{\circ}\text{C}$  average of  $\sim 0.03^{\circ}\text{C/hr}$  can be deduced.



Sketches (from photomicrographs) of two examples, in a thin section (15058, 127) of an Apollo 15 mare basalt, of the textural relationships of zoned clinopyroxenes (white, subophitic and twinned in I; white, ophitic in II) and zoned plagioclase (dashed). The numbers or letters (C, M,  $M_1$  refer to pyroxene II) correspond approximately with microprobe analyses in the positions shown in these sketches; arrows indicate in the quadrilateral the inferred directions of crystal growth; cr-cristobalite, opaques omitted. In pyroxene II the position of the second three determinations only approximately coincided with the first three but are given the same lettering (C, M,  $M_1$ ). The area hachured is the approximation to the pyroxene composition at the time when plagioclase began to crystallize, inferred from the textural relations. Two independent series of microprobe analyses on these pyroxenes were made as a check on accuracy.

Figure 9. Radial growth in 15058,127  
(Donaldson et al., 1977).

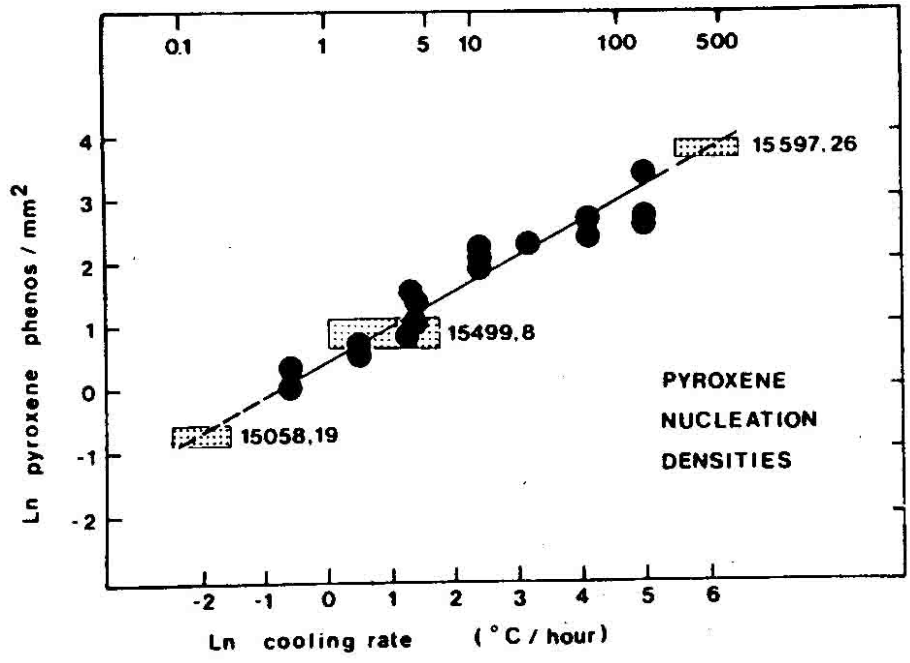


Figure 10. Pyroxene nucleation density/cooling rate (Grove and Walker 1977).

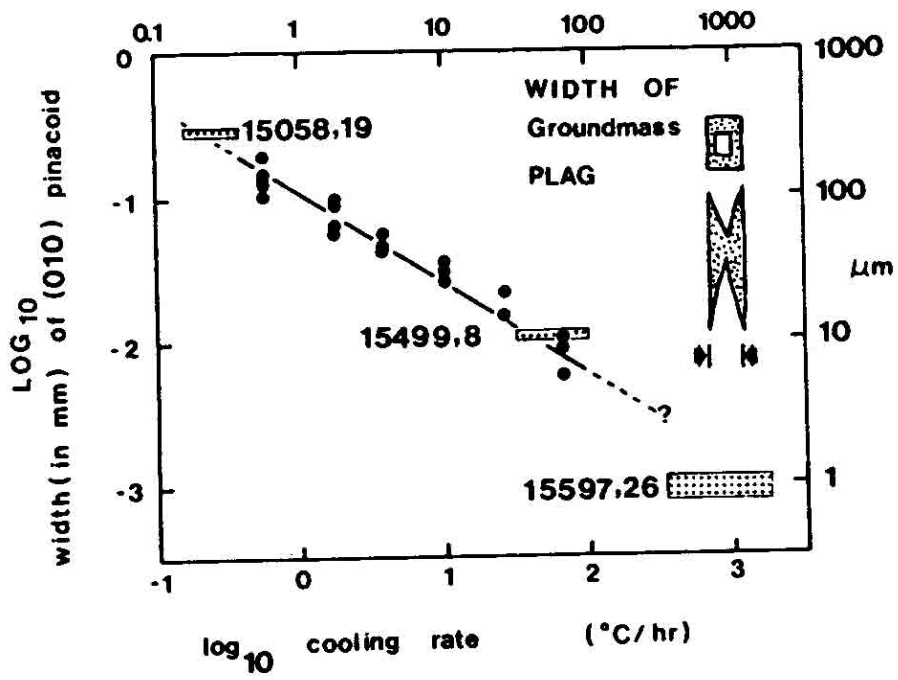
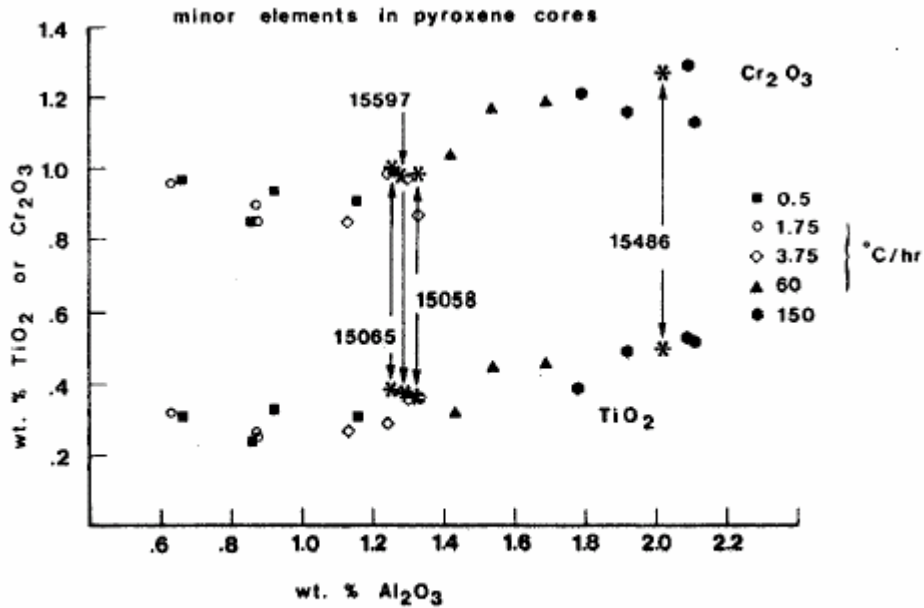


Figure 11. Plagioclase "size"/cooling rate (Grove and Walker 1977).



Comparison of minor element contents of pyroxene cores in Apollo 15 quartz-normative basalts with the pyroxene cores of the controlled cooling rate experiments. Weight percent Al<sub>2</sub>O<sub>3</sub> is plotted against wt.% TiO<sub>2</sub> and Cr<sub>2</sub>O<sub>3</sub>. Asterisks indicate lunar samples and other symbols indicate the cooling rate experiments.

Figure 12. Minor elements in pigeonite cores/cooling rate (Grove and Bence 1977).

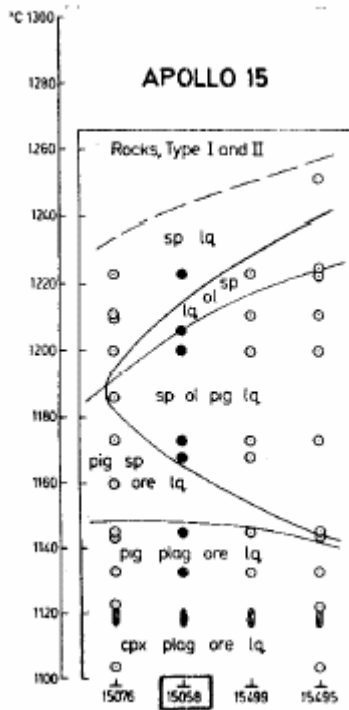


Figure 13. Low-pressure relationships (black dots) (Humphries et al., 1972).

TABLE 15058-3.

Wt %	,39	,76	,5	,9	,76	WR	,4	,86	,74	,72	,95	,32
B102	48.47	46.7	47.81									
TiO2	1.60	2.3	1.77	1.80								
Al2O3	8.90	9.1	8.87	9.3								
FeO	19.75	19.1	19.97	20.1	19.5							
MgO	9.56	10.8a	9.01									
CaO	10.23		10.32									12.3
Na2O	0.28		0.28	0.2957								
K2O	0.038		0.03			0.0486						0.0642
P2O5	0.049		0.08									
(ppm) Sc				46	42							
V												
Cr	4600			2865	2840			5870,3800,4790				
Mn	2120	2600	2200									
Co				42								
Ni												
Rb	<2											
Sr	99.2											
Y	21.1											
Zr	70.9				74,97b							
Nb	4.9											
Hf				2.6	1.80,2.52							
Ba	49											
Th						0.52						
U						0.13						
Pb												
La				6.0								
Ce												
Pr												
Nd												
Sm				4.1								
Eu				1.08	0.96							
Gd												
Tb				0.9								
Dy												
Ho												
Er												
Tm												
Yb				2.5								
Lu				0.43								
Li												
Be								0.45				
B												
C						27	27		10			
N												
S	570		700						970	950		
F												
Cl												
Br												
Cu												
Zn												
(ppb) I												
At												
Ga												
Ge												
As												
Se												
Mo												
Tc												
Ru												
Rh												
Pd												
Ag												
Cd												
In												
Sn												
Sb												
Te												
Cs												
Ta				460								
W												
Re												
Os												
Ir												
Pt												
Au												
Hg												
Tl												
Bi												
	(1)	(2)	(3)	(4)	(5)	(6)	(7)	(8)	(9)	(10)	(11)	(12)

TABLE 15058-3 Continued

	,85	,209	,207
Wt % SiO <sub>2</sub>			
TiO <sub>2</sub>			
Al <sub>2</sub> O <sub>3</sub>			
FeO			
MgO			
CaO			
Na <sub>2</sub> O			
K <sub>2</sub> O	0.0398		
P <sub>2</sub> O <sub>5</sub>			
(ppm) Sc			
V			
Cr			
Mn			
Co			
Ni		0.50	
Rb	0.811c	0.646	
Sr	99.5d		
Y			
Zr			
Nb			
Hf			
Ba			
Th			
U		0.089	
Pb			
La			
Ce			
Pr			
Nd			
Sm			
Eu			
Gd			
Tb			
Dy			
Ho			
Er			
Tm			
Yb			
Lu			
Li			
Be			
B			
C			5.3e
N			<0.1
S			671
F			
Cl			
Br			
Cu			
Zn		0.94	
(ppb) I			
At			
Ga			
Ge		6.47	
As			
Se		56	
Mo			
Tc			
Ru			
Rh			
Pd		<0.51	
Ag		0.27	
Cd		3.35	
In		0.40	
Sn		83	
Sb		0.43	
Te		2.0	
Cs		26.7	
Ta			
W			
Re		0.0006	
Os		<0.02	
Ir		0.0063	
Pt			
Au		0.081	
Hg			
Tl		0.22	
Bi		<0.17	
	(13)	(14)	(15)

References to Table 15058-3

References and methods:

- (1) Willis et al. (1972); XRF
- (2) Janghorbani et al. (1973); NAA
- (3) Rhodes and Hubbard (1973); PET (1972); XFR/AA
- (4) Fruchter et al. (1973); INAA
- (5) Ehmman et al. (1975); INAA, RNAA
- (6) O'Kelley et al. (1972); -ray
- (7) Desmarais et al. (1972); Combustion
- (8) Moore et al. (1972); Combustion
- (9) Eisentraut et al. (1972)
- (10) Moore et al. (1973); Combustion
- (11) Gibson et al. (1975); Combustion, hydrolysis
- (12) Husain (1974); MS
- (13) Birck et al. (1975); ID/MS
- (14) Wolf et al. (1979); RNAA
- (15) Desmarais (1978); Temp. releases

Notes:

- (a) Authors reservation on accuracy.
- (b) Averaged and corrected to 84.1 ppm by Garg and Ehamnn (1976)
- (c) Calc. from <sup>87</sup>Rb.
- (d) Calc. from <sup>86</sup>Sr.
- (e) Only 2.5 ppm indigenous.

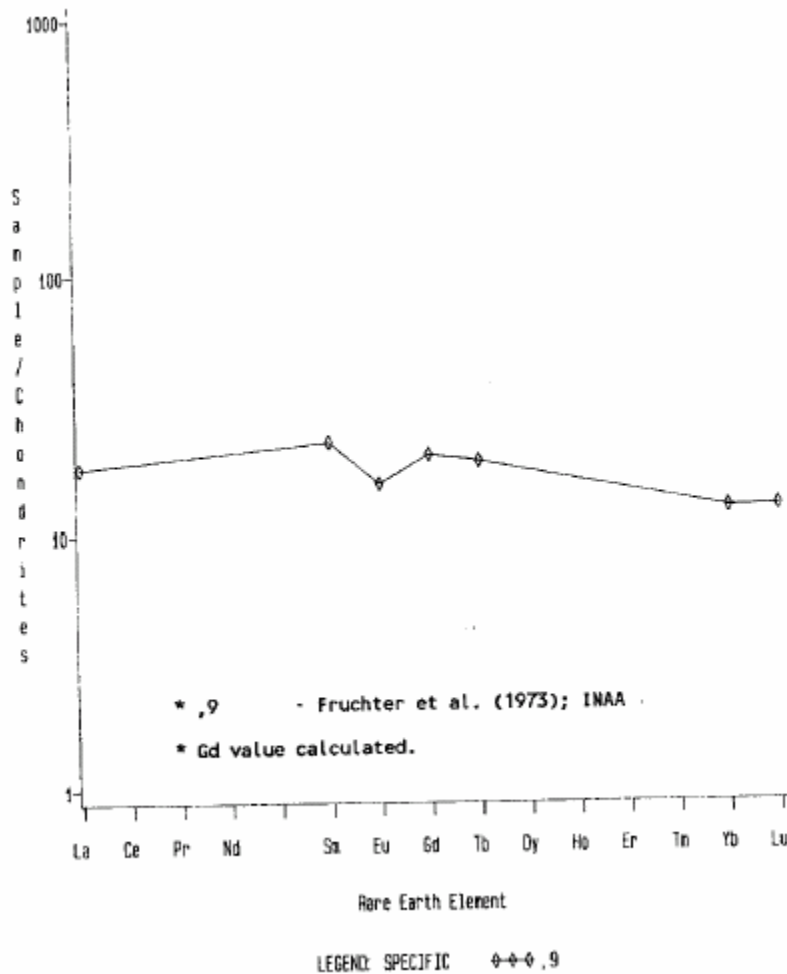


Figure 14. Rare earths in bulk rock.

**EXPERIMENTAL PETROLOGY:** While experiments on the near isochemical sample 15597 (e.g., Bence and Grove 1977) are relevant, little experimental data for 15058 rock powders themselves are available. Humphries et al. (1972) briefly report the results of equilibrium, low-pressure experiments on 15058 (Fig. 13), and these results are shown in various projections by O'Hara and Humphries (1977). The sample crystallizes a little olivine prior to pigeonite entry, and the olivine is resorbed before plagioclase crystallizes. They claim there is little iron loss in their experiments. As for other Apollo 15 quartz normative basalt samples, Humphries et al. (1972) prefer the hypothesis that 15058 is a pyroxene cumulate from a cotectic (px + pl) liquid, and was erupted at  $\sim 1150^{\circ}\text{C}$ , not the  $\sim 1220^{\circ}\text{C}$  liquidus of the experiments (see Walker et al., 1977 for the case against this hypothesis).

**CHEMISTRY:** Published chemical analyses are listed in Table 3. While comprehensive, there is not much duplication for minor elements; only one set of rare-earth data exists

(Fig. 14). Little specific comment on the analyses exist other than to note the similarity with other Apollo 15 quartz-normative basalts. Gibson et al. (1975) note that sulfur abundances measured following hydrolysis are lower than those following combustion, presumably because some sulfur is in an acid-resistant phase. Desmarais (1978) using a more refined method, found much lower carbon than in previous analyses and concluded (partly from isotopic analyses) that the carbon released at low temperature is a terrestrial contaminant. Apart from the data in Table 3, 12 micron moles H/gm were found by Desmarais et al. (1974); 17.4 and 21.2 ppm H by Gibson et al. (1975); and Janghorbani et al. (1973) analyzed for O (38.6%). Desmarais (1978) also quotes S=400 ppm in an unpublished check list of Moore. Oxides of carbon and CH<sub>4</sub> data were presented by Gibson and Moore (1972), Gibson et al. (1975) and Desmarais et al. (1972).

Wolf and Anders (1980) quoted 15058 as a mare basalt with an atypically low Se content, a characteristic correlated with low U and Rb, and suggestive that the source reservoir has too little S and Se to be saturated with a sulfide at large degrees of partial melting.

Sato (1973) measured the oxygen fugacity in two splits over a range of temperatures, finding values (Fig. 15, Table 4) similar to other mare basalts and midway between the iron-wustite and iron-rutile-ferropseudobrookite buffers.

STABLE ISOTOPES: Epstein and Taylor (1972) reported oxygen and silicon isotopic analyses (Table 5) for mineral separates. The data show no unusual characteristics; the plagioclase-clinopyroxene difference is similar to other lunar basalts and appropriate for magmatic temperatures. Gibson et al. (1975) reported  $^{34}\text{S}_{\text{CDT}0/00} = -0.5$  and  $-0.6$  for two splits. Desmarais (1978) reported  $^{13}\text{C}$  data, finding a variation from  $-33.1\%$  for a  $420^\circ\text{C}$  release to  $-3.3\%$  for a  $1270^\circ\text{C}$  release. The lower temperature carbon is similar to terrestrial cloth fibers and plastics, etc. Assessing the possibility of spallation produced  $^{13}\text{C}$  (because the high temperature value is high), Desmarais calculates a spallation age of 470 m.y., assuming original  $^{13}\text{C} = -20$ .

RADIOGENIC ISOTOPES AND GEOCHRONOLOGY: Birck et al. (1975) determined a Rb-Sr internal isochron with an age of  $3.46 \pm 0.07$  b.y. and initial  $^{87}\text{Sr}/^{86}\text{Sr}$  of 0.69928 (Fig. 16, Table 6). They discuss and conclude they cannot deny the possibility that the "isochron" is a mixing line.

Husain (1974) found a good high temperature Ar-Ar plateau corresponding to an age of  $3.358 \pm 0.025$  b.y. (Fig. 17), although significant radiogenic  $^{40}\text{Ar}$  has been lost from the samples (variously stated as 7.5%, 8.6%, and 8.9% in the paper; 9% in Husain, 1972). This loss leads to a lower K-Ar age of  $3.213 \pm 0.015$  b.y.

RARE GASES, EXPOSURE AND TRACKS: Husain (1974) tabulates an exposure age of  $135 \pm 7$  m.y. derived from high temperature ( $>1000^\circ\text{C}$ ) Ar releases. Eldridge et al. (1972) list  $^{22}\text{Na}$ ,  $^{26}\text{Al}$ , and  $^{54}\text{Mn}$  data without specific discussion. The data are similar to that for (near-isochemical) 15065 in which  $^{22}\text{Na}$  and  $^{26}\text{Al}$  appear to be saturated, and 15058 is listed as saturated with  $^{26}\text{Al}$  by Yokoyama et al. (1974). Thus 15058 has been exposed for at least  $\sim 2$  m.y.

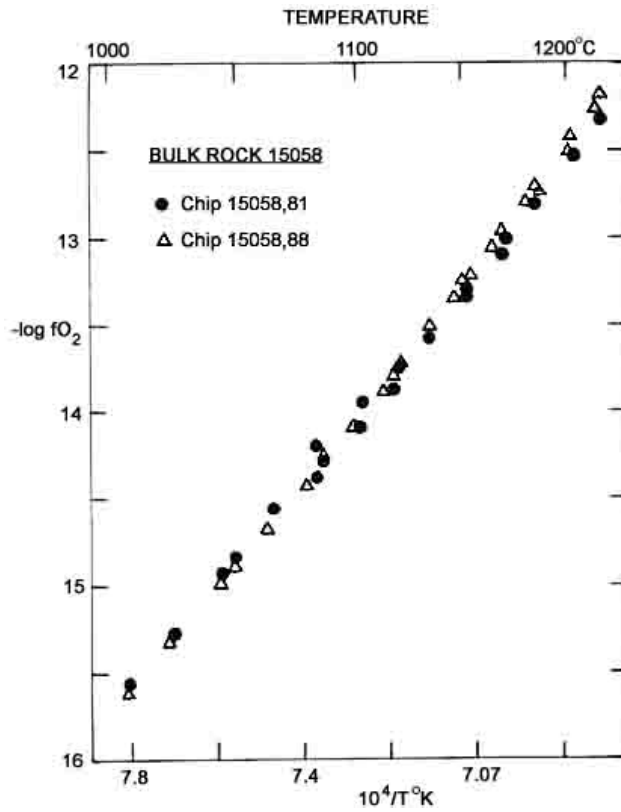


Figure 15.  $f_{O_2}$  of two chips measured separately (Sato et al., 1973).

TABLE 15058-4. Oxygen fugacity ( $-\log f_{O_2}$ ) as a function of temperature (Sato et al., 1973)

	1000°C	1050°C	1100°C	1150°C	1200°C
15058,81	15.7	14.9	14.0	13.3	12.6
15058,88	15.7	14.9	14.0	13.3	12.5

TABLE 15058-5. O and Si isotopic data (Epstein and Taylor, 1972)

	$\delta O^{18}$	$\delta Si^{30}$
cpx	$5.73 \pm 0.04$	$-0.31 \pm 0.05$
pl	$6.13 \pm 0.05$	$-0.14 \pm 0.10$

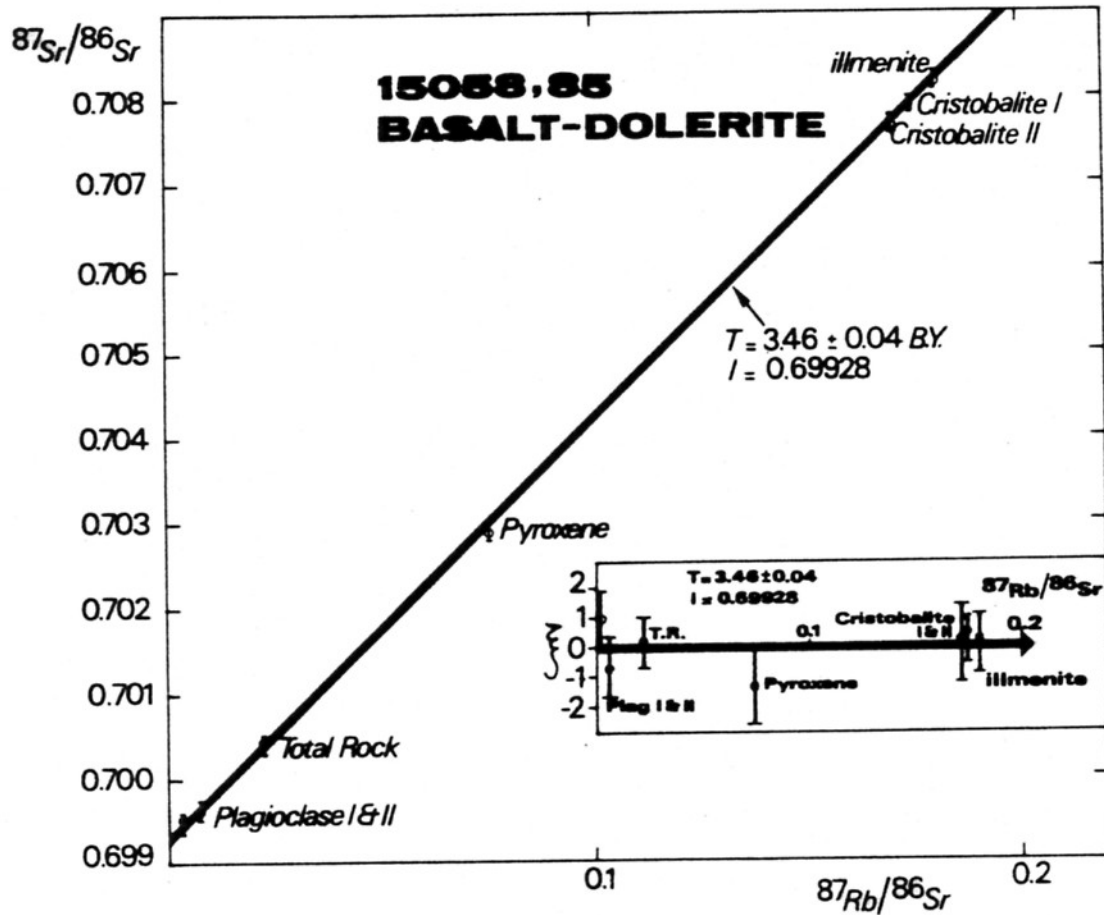
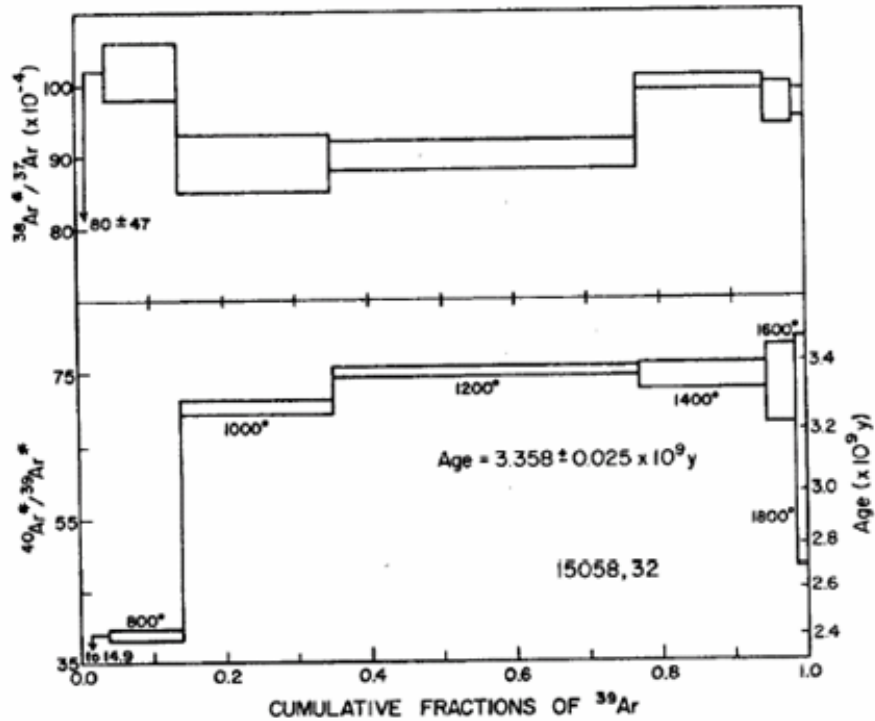


Figure 16. Rb-Sr internal isochron  
(Birck et al., 1975).

TABLE 15058-6. K, Rb, Sr concentrations and isotopic composition for 15058,85 (Birck et al., 1975)

Samples	Weight (mg)	K (ppm)	$^{87}\text{Rb}$ (ppm)	$^{86}\text{Sr}$ (ppm)	$^{87}\text{Rb}/^{86}\text{Sr}^1$	$^{87}\text{Sr}/^{86}\text{Sr}^{2,3}$
<i>15058,85</i>						
Total rock	26.7	332	0.2254	9.85	0.02262	0.70040 (6)
Plagioclase	38.3	545	0.1197	35.9	0.00320	0.699507 (60)
Plagioclase	31.2	605	0.297	40.44	0.0073	0.69659 (7)
Pyroxene	12.9	143	0.1364	1.800	0.0749	0.70288 (9)
Cristobalite	2.7	2275	1.361	7.715	0.1743	0.70789 (5)
Ilmenite	3.2	367	0.366	2.005	0.1804	0.70818 (7)
Cristobalite	1.5	3360	1.416	1.416	8.223	0.70767 (8)



Comparison of the  $^{40}\text{Ar}^*/^{39}\text{Ar}^*$  and  $^{36}\text{Ar}^*/^{37}\text{Ar}^*$  release diagrams for crystalline rock 15058.32. The 1000° and 1200°C fractions show an  $^{40}\text{Ar}^*/^{39}\text{Ar}^*$  plateau. The 1200°C and higher-temperature fractions exhibit an  $^{36}\text{Ar}^*/^{37}\text{Ar}^*$  plateau typical of many lunar basalts.

Figure 17. Ar release diagram (Husain, 1974).

Track determinations result in lower ages. Bhandari et al. (1972, 1973) illustrate the track density/depth profile, which is steep at depths less than 0.1 cm (Fig. 18). A suntan age (2 m.y.) is lower than the subdecimeter age (10 m.y.) and illustrates a multiple history; the low suntan age probably results from the friability of the rock, as with other Apollo 15 samples. Poupeau et al. (1972) studied tracks and produced a density vs. depth profile for feldspar. The lunar top-face showed no solar flare irradiation, in contrast with the bottom, which gives an exposure age of  $\frac{1}{2}$  - 2 m.y. Generally the track density is low, and in the outer millimeter variable because of erosion differences. Galactic tracks have a flat profile with little variation, indicating that most were registered under heavy shielding. Crozaz et al. (1974) in tabulating exposure ages for 15058 (and other rocks), list a "single-point determination" of 25 m.y., referencing Poupeau et al. (1972) as the source. Fleischer et al. (1973) studied track densities in located samples. Olivine has a low density, probably because some heating event has erased tracks--the relevant shock event was less than 7 m.y. ago. Short tracks, if produced by spallation, suggest a near-surface age of a few hundred million years; cosmic ray track densities require 2,000 m.y. under 10 cm of cover or a few hundred million years at shallower depth, suggesting a long near-surface exposure history prior to the 7 m.y. track-erasing event. Crozaz et al. (1974) tabulate a 10 m.y. "single point determination" unpublished data by Yuhas.

**PHYSICAL PROPERTIES:** Nagata et al. (1972a,b, 1973, 1975) tabulate basic magnetic data and the results of NRM determinations from demagnetization (Fig. 19). 15058 has a hard component of NRM  $\sim 1 \times 10^{-6}$  emu/gm, with a direction which is reasonably invariant for fields greater than 100 Oe.rms. TRM demagnetizing experiments suggest that the NRM is attributable to a TRM acquired by cooling from at most 300°C. If the stable component of NRM can be attributed to PTRM, the ambient lunar magnetic field is estimated to be 2,000. Banerjee and Mellema (1974) used an ARM method and determined a field of 4,900 a result which Collinson et al. (1975) suggested must be treated with caution: the method is valid for single domain grains whereas lunar mare basalts are dominantly multidomain. Schwerer et al. (1974) determined the variation of electrical conductivity with temperature (Fig. 20). They found large decreases in conductivity following heating in reducing atmospheres, a process which produces Fe-metal (they also show Mossbauer spectra).

Schwerer et al. (1974) note that Housley, in a review of the paper, suggested that the low conductivity of 15058 might result from its high porosity and its high density of microcracks.

Mitzutani and Newbigging (1973) list a density of 2.99 gm/cc and measurements of velocity as a function of pressure are tabulated as depicted (Fig. 21, Table 7). At high pressures 15058 is seismically similar to other rocks.

Charette and Adams (1975) depict the spectra from 0.5-2.5 microns for a powdered sample of 15058. It has a typical quartz normative basalt pattern, with a narrow pyroxene band not widened by the presence of olivine.

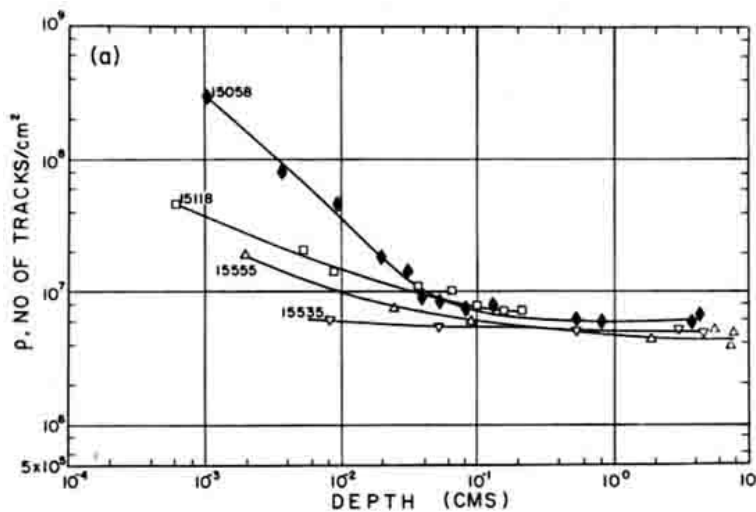
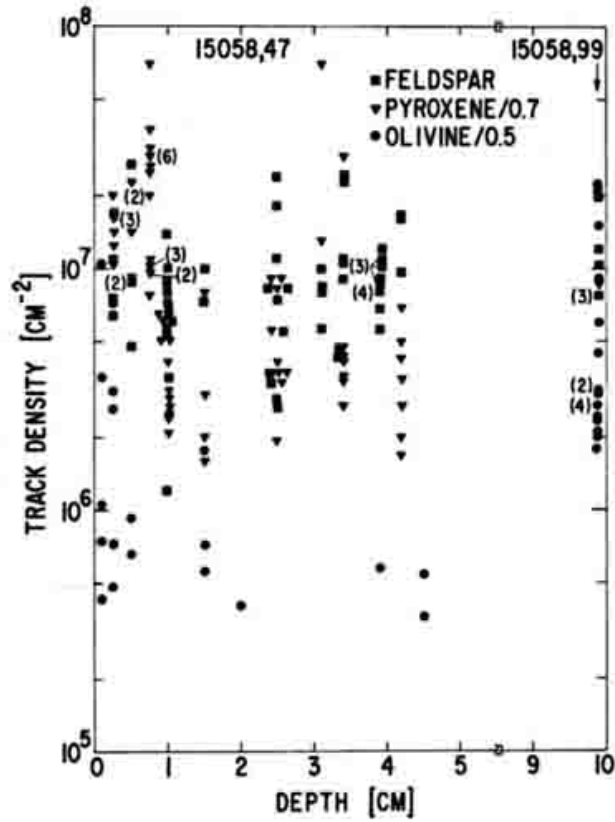
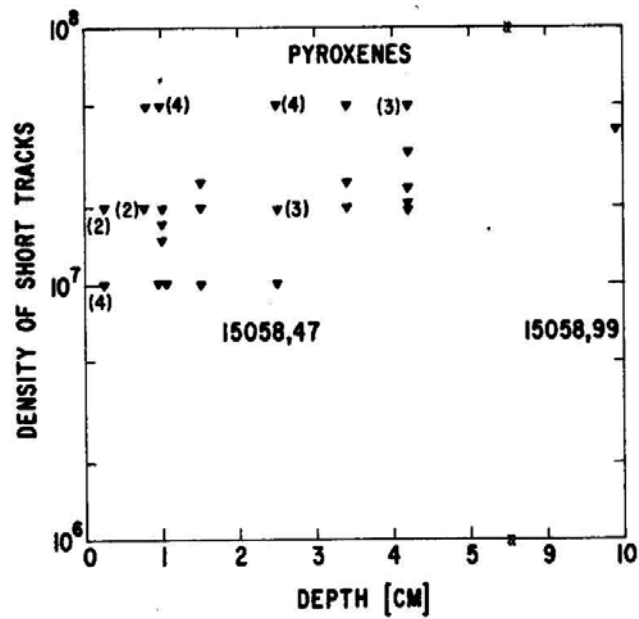


Fig. 18a



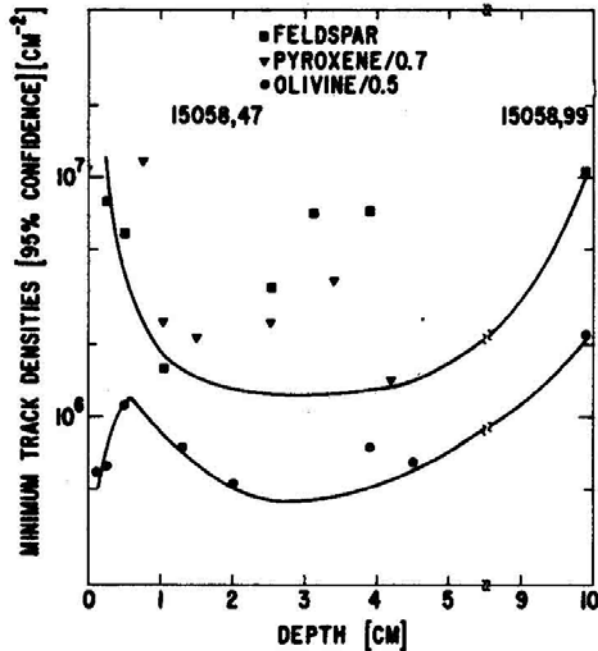
Track densities observed in individual crystals of three different minerals of 15058,47 and 15058,99. The pyroxenes show evidence of shock.

Fig. 18b



Density of short tracks ( $\approx 1.5 \mu$  in length) in pyroxenes from 15058.

Fig. 18c



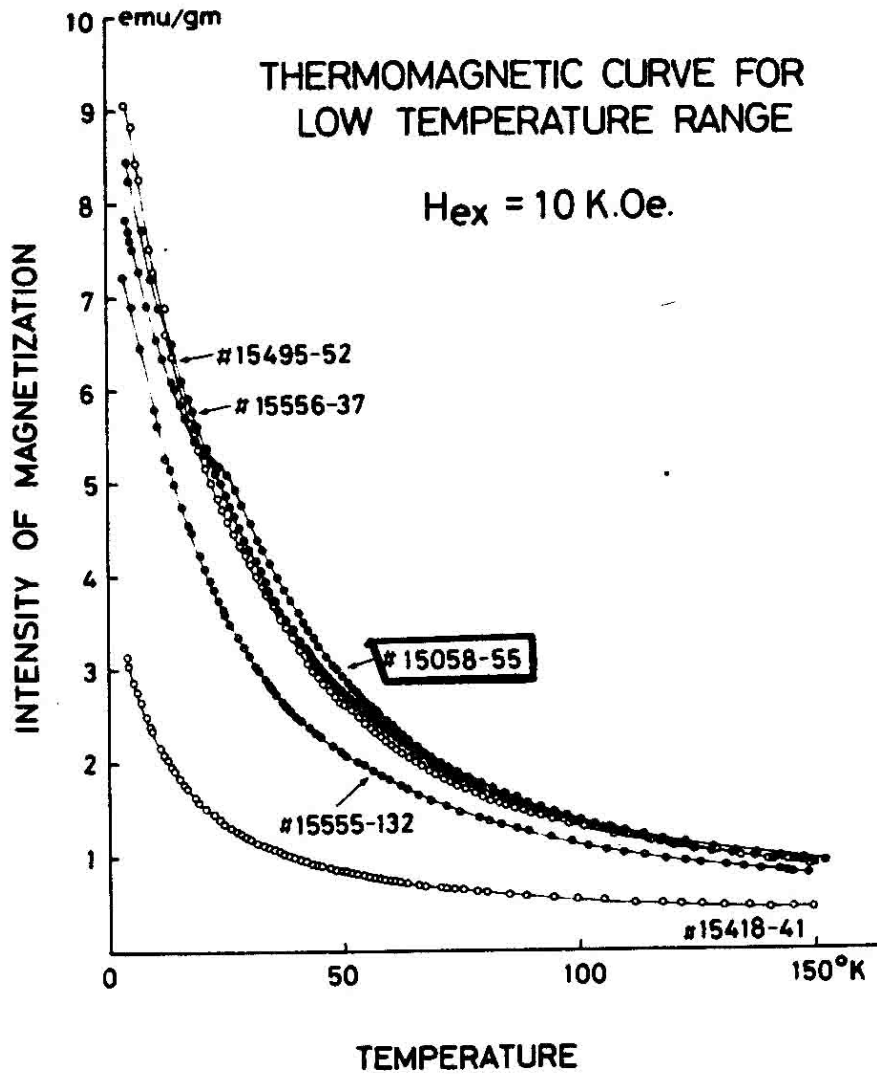
Minimum track densities (95% confidence) at each position sampled in 15058. Curves show the smoothed lower limits for feldspars plus pyroxenes and for olivines.

Fig. 18d

Figure 18. Track density studies  
 (a) Bhandari et al. (1973), black diamonds;  
 (b)-(d) Fleischer et al. (1973).

PROCESSING AND SUBDIVISIONS: Following chipping of a few exterior fragments, 15058 was substantially sawn (Fig. 22). The interior slab ,24 and the orthogonal slab pieces ,27 (now 53 g) and ,30 (now 102 g) were substantially subdivided. ,29 (originally 558 g) has been totally subdivided, mainly into four large pieces >100 g, for PAO exhibits. The remaining large pieces ,26 (337 g), ,28 (321 g), and ,31 (620 g, in BSV) remain intact.

Thin sections were made from exterior chips (,11 and ,12) from the E face, and from ,60, a portion of the interior slab ,24 (Fig. 22).



Thermomagnetic curves of Apollo 15 samples in a temperature range between 4.2°K and 150°K.

Figure 19. Thermomagnetic curve for 15058 and other Apollo 15 samples (Nagata et al., 1973).

TABLE 15058-7.  $V_p$  v. Pressure (Mizutani and Newbigging, 1973)

Kb	0.0	0.5	1.0	2.0	3.0	5.0	7.0	9.0
$V_p$ (km/spc)	4.03	5.33	5.54	5.85	6.12	6.49	6.65	6.73

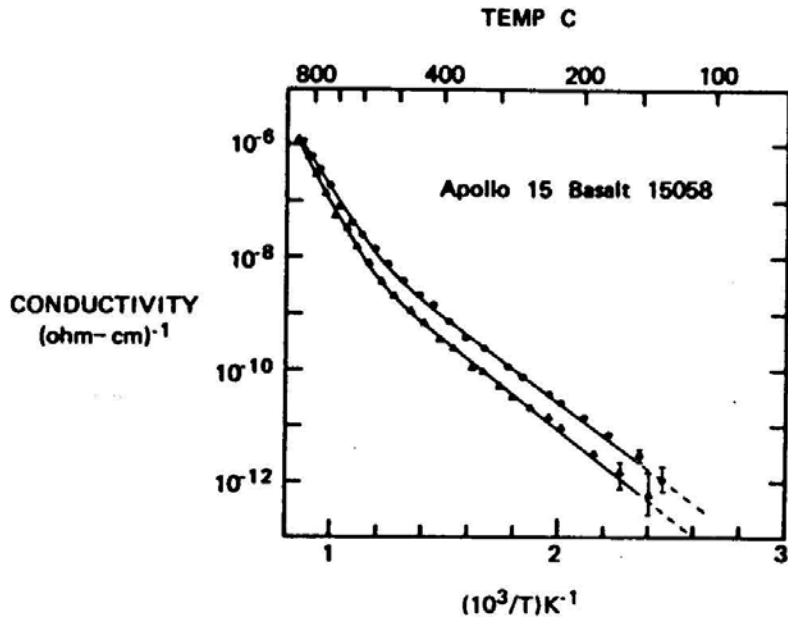


Figure 20. Conductivity vs. temperature (Schwerer et al., 1974).

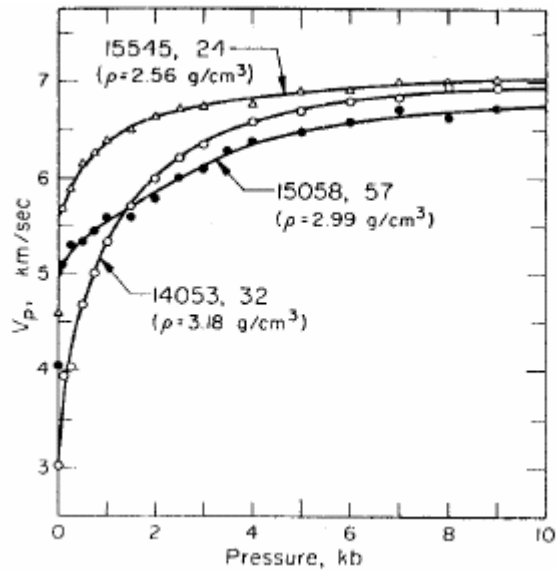


Figure 21. Seismic velocity vs. pressure (Mizutani and Newbigging, 1973,

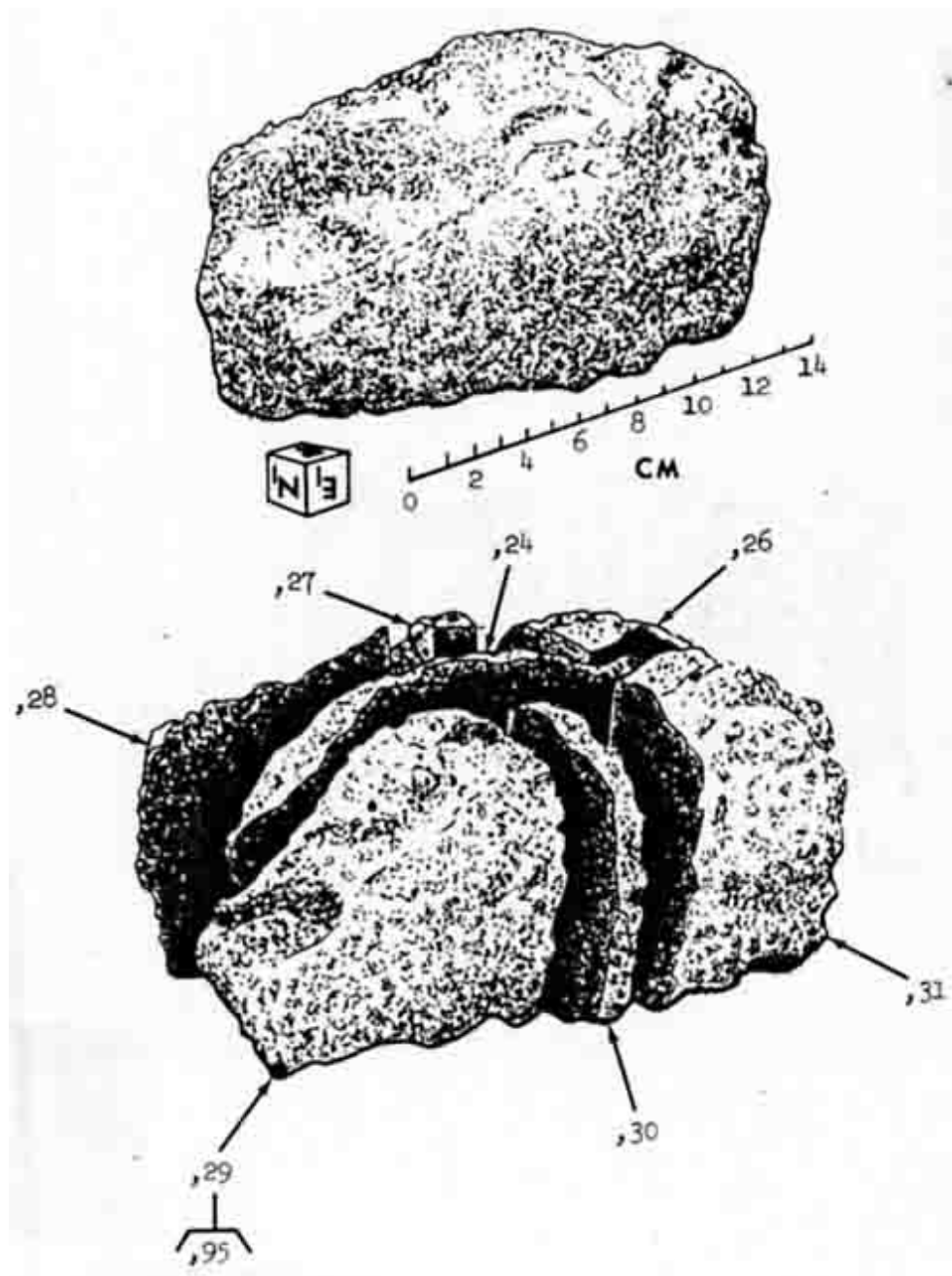


Figure 22. Main subdivision of 15058.